Paweł MARTYNOWICZ*, Bogdan SAPIŃSKI*

EXPERIMENTAL STUDY OF VIBRATION CONTROL IN A TWO-DEGREE-OF-FREEDOM PITCH-PLANE MODEL OF A MAGNETORHEOLOGICAL VEHICLE SUSPENSION

SUMMARY

The paper concerns the vibration control in a two-degree-of-freedom model of vehicle suspension equipped with independently controlled MR dampers in front and rear sections. The suspension model was tested in open-loop and feedback system configurations under harmonic and square base excitations. The experiments were conducted on the specially designed laboratory setup with data acquisition and control system configured in MATLAB/Simulink environment. The obtained results reveal effectiveness of MR dampers in vibration isolation for a wide range of excitation frequencies.

Keywords*: MR damper, pitch-plane suspension model, vibration control*

STEROWANIE DRGANIAMI PŁASKIEGO MODELU MAGNETOREOLOGICZNEGO ZAWIESZENIA POJAZDU O DWÓCH STOPNIACH SWOBODY – BADANIA EKSPERYMENTALNE

W artykule poruszono zagadnienie sterowania drganiami płaskiego modelu zawieszenia pojazdu o dwóch stopniach swobody, wyposażonego w niezależnie sterowane tłumiki MR w części przedniej i tylnej. Model zawieszenia badano w układzie otwartym oraz zamkniętym, przy harmonicznych oraz prostokątnych wymuszeniach podłoża. Badania eksperymentalne prowadzono z wykorzystaniem specjalnie zaprojektowanego stanowiska laboratoryjnego wyposażonego w aparaturę pomiarowo-sterującą współpracującą z środowiskiem MATLAB/Simulink. Uzyskane rezultaty potwierdzają efektywność tłumików MR w zakresie redukcji drgań rezonansowych oraz nadrezonansowych.

Słowa kluczowe*: tłumik MR, płaski model zawieszenia, sterowanie drganiami*

1. INTRODUCTION

The suspensions in automotive, off-road machinery, railway are designed in order to isolate the sprung mass (drivers, operators, passengers) from the vibration caused by the road unevenness. The performance of a passive vehicle suspension is always limited by the trade-off between comfort level and drive stability, resulting from the fixed parameters of the suspension, established by the designer. These parameters are a result of the optimization of the above opposing goals. Hence the ability of the designed passive suspension to store energy via a spring and to dissipate via a damper results in the characteristics determined by the system stiffness and damping. To solve the problem of unavoidable compromise accompanied passive suspensions, active and semi-active (e.g. magnetorheological, MR) suspensions have been proposed.

The review of simple but credible models that can be useful for fundamental vibration analysis in terms of resonant frequencies and forced vibration response of sprung and unsprung masses reveals that the vibration response of vehicles to various excitations can be investigated through the analysis of in-plane models [1, 8, 9, 17]. Because the wheelbase of the majority of ground vehicles is significantly larger than the track width, the roll motions are often considered negligible. That is why we consider a pitch-plane model of a vehicle suspension. We assume negligible contributions due to tires damping, and tires stiffness that is 6–10 times higher than that of primary suspension (the road input is taken to be the same as the wheels input). Such model is considered applicable for study of off-road vehicles without tires (trains, caterpillar vehicles: excavators, tanks, etc.) or without primary suspension – then stiffness and damping factors apply to the tires properties alone. The investigation of a pitch-plane model enables us to observe such dynamic system properties as vibration modes and resonant frequencies.

In the paper we will present results of experimental analysis conducted on a specially designed and built laboratory setup of pitch-plane model of MR vehicle suspension. The measurement and control system is supported by MATLAB/Simulink environment. We demonstrate suspension performance improvements obtained through the control of MR dampers. The experimental study described in this paper was preceded by the numerical simulations presented in [5, 6, 11, 12].

2. MATHEMATICAL MODEL

Let us consider a pitch-plane model of a vehicle suspension system shown in Figure 1. The suspension model comprises a stiff beam with the mass m and the moment of inertia J with regard to beam's centre of gravity (cog) P_g, supported jointly at points P_f, P_r on identical spring – MR damper sets. The system has two degrees of freedom: vertical displacement x and longitudinal bounce φ at P_g. Technically, two degrees of freedom are ensured by applying rigid stabilizing vertical guides positioned symmetrically on two sides of the beam (to restrict the motion of the beam's cog). The beam is base-excited by the displacements w_f, w_r.

* Department of Process Control, AGH University of Science and Technology; pmartyn@agh.edu.pl; deep@agh.edu.pl

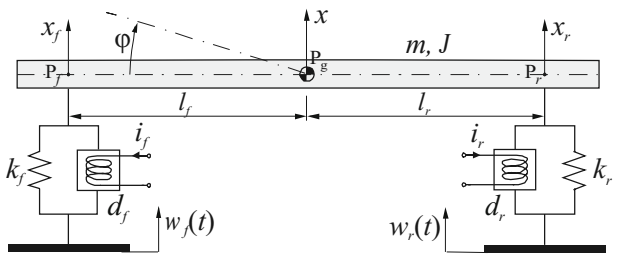

Fig. 1. Pitch-plane model of a vehicle suspension system

We assume that distance $l_f + l_r$ is large in relation to the maximal amplitude of vertical displacement of the beam's cog. Introducing equations that govern the dynamics of the system from Figure 1 we assume that sinφ = φ, which make reasonable equations (2.1), (2.2):

$$x_f = x + l_f \varphi \tag{2.1}$$

$$x_r = x - l_r \varphi \tag{2.2}$$

Denoting resultant forces acting on the front and rear sections of the beam by F_f, F_r we get:

$$F_f = F_{kf} + F_{df} \tag{2.3}$$

$$F_r = F_{kr} + F_{dr} \tag{2.4}$$

where F_{kf}, F_{kr} are elasticity forces given by:

$$F_{kf} = -k_f (x_f - w_f) \tag{2.5}$$

$$F_{kr} = -k_r (x_r - w_r) \tag{2.6}$$

and F_{df}, F_{dr} are dampers forces in front and rear sections respectively. These forces can be expressed using Spencer model for fluctuating magnetic fields [14].

When we neglect the gravity forces of the beam and associated deflection of springs and dampers, the displacements x, φ in the steady state shall be both equal to zero. Accordingly, the equation the suspension system dynamics can be written as:

$$m\ddot{x} = F_f + F_r \tag{2.7}$$

$$J\ddot{\varphi} = F_f l_f - F_r l_r \tag{2.8}$$

Substituting equations (2.1)–(2.6) into (2.7) and (2.8), we get the model of the suspension system in the form:

$$\ddot{x} = -\frac{k_f + k_r}{m} x - \frac{k_f l_f - k_r l_r}{m} \varphi + \frac{k_f}{m} w_f + \frac{k_r}{m} w_r + \frac{1}{m} F_{df} + \frac{1}{m} F_{dr} \tag{2.9}$$

$$\ddot{\varphi} = -\frac{k_f l_f - k_r l_r}{m} x - \frac{k_f l_f^2 + k_r l_r^2}{J} \varphi + \frac{k_f l_f}{J} w_f - \frac{k_r l_r}{J} w_r + \frac{l_f}{J} F_{df} - \frac{l_r}{J} F_{dr} \tag{2.10}$$

Assuming that $k_f = k_r = k$ and converting equations (2.9) and (2.10) we obtain the following state space representation of the system:

$$\dot{\boldsymbol{X}} = \boldsymbol{A} \cdot \boldsymbol{X} + \boldsymbol{B} \cdot \boldsymbol{U} \tag{2.11}$$

$$\boldsymbol{Y} = \boldsymbol{C} \cdot \boldsymbol{X} \tag{2.12}$$

where:

$$\boldsymbol{X} = \left[x \quad \dot{x} \quad \varphi \quad \dot{\varphi}\right]^T \tag{2.13}$$

$$\boldsymbol{U} = \left[F_{df} + k w_f \quad F_{dr} + k w_r\right]^{\mathrm{T}} \tag{2.14}$$

$$\boldsymbol{A} = \begin{bmatrix} 0 & 1 & 0 & 0 \\ -\frac{2k}{m} & 0 & -k\frac{l_f - l_r}{m} & 0 \\ 0 & 0 & 0 & 1 \\ -k\frac{l_f - l_r}{J} & 0 & -k\frac{l_f^2 + l_r^2}{J} & 0 \end{bmatrix} \qquad \boldsymbol{B} = \begin{bmatrix} 0 & 0 \\ \frac{1}{m} & \frac{1}{m} \\ 0 & 0 \\ \frac{l_f}{J} & -\frac{l_r}{J} \end{bmatrix} \tag{2.15}$$

$$\boldsymbol{Y} = \begin{bmatrix} x \\ \varphi \end{bmatrix} \qquad \boldsymbol{C} = \begin{bmatrix} 1 & 0 & 0 & 0 \\ 0 & 0 & 1 & 0 \end{bmatrix} \tag{2.16}$$

Equation (2.11) is a state space representation of the pitch-plane model of a vehicle suspension system. This representation will be taken into account in further considerations. Note, that state variable vector $\boldsymbol{X}$ includes displacements x and φ, and velocities $\dot{x}$ and $\dot{\varphi}$, while input vector $\boldsymbol{U}$ includes respective sums of dampers forces F_{df} and F_{dr}, and elasticity forces due to base displacements w_f and w_r.

We assumed the following model parameters: distance l_f = 0.7 m, distance l_r = 0.7 m, total length of the beam L = 1.5 m, width of the beam a = 0.173 m, height of the beam b = 0.124 m, mass of the beam m = 253.68 kg, moment of inertia of the beam J = 49.20 kgm^2, stiffness factor of the front (rear spring) $k_f = k_r$ = 42 016 N/m.

3. CONTROL ALGORITHMS

We introduce three control algorithms for MR dampers in the controlled vehicle suspension system. These algorithms are denoted by CA1, CA2, CA3. The algorithms were developed in order to minimize vertical and angular accelera-

tions (i.e. to minimize the relevant vibration transmission coefficients in the system). The algorithms determine the optimal (in the context of the applied criterion) instantaneous values of damper forces F_{df}^* and F_{dr}^*, and reference currents i_f^* and i_r^*, for which the damper forces reach the values as close as possible to F_{df}^* and F_{dr}^*.

The CA1 is a semi-active realization of skyhook control by the use of MR dampers; it indicates how to modulate the MR dampers that they emulate skyhook dampers. The CA2 also employs the skyhook concept while the CA3 applies LQ concept. The CA2 and CA3 are applied in conjunction with the inverse model of MR damper introduced in [6, 13].

In accordance with [2], conditions determining the optimal values of skyhook dampers' forces are given by:

$$F_{df}^* = \begin{cases} -c_{sky}\dot{x}_f, & \dot{x}_f\left(\dot{x}_f - \dot{w}_f\right) \geq 0 \\ 0, & \dot{x}_f\left(\dot{x}_f - \dot{w}_f\right) < 0 \end{cases} \tag{3.1}$$

$$F_{dr}^* = \begin{cases} -c_{sky}\dot{x}_r, & \dot{x}_r\left(\dot{x}_r - \dot{w}_r\right) \geq 0 \\ 0, & \dot{x}_r\left(\dot{x}_r - \dot{w}_r\right) < 0 \end{cases} \tag{3.2}$$

Algorithm CA1 is based on equations (3.1) and (3.2). Utilizing the skyhook concept, this algorithm defining the reference current levels i_f^* and i_r^* at which the dampers generate force values F_{df}^* and F_{dr}^* can be rewritten as:

CA1:
$$i_f^* = \begin{cases} i_{fo}\left|\dot{x}_f\right|, & \dot{x}_f\left(\dot{x}_f - \dot{w}_f\right) \geq 0 \\ 0, & \dot{x}_f\left(\dot{x}_f - \dot{w}_f\right) < 0 \end{cases}$$
$$i_r^* = \begin{cases} i_{ro}\left|\dot{x}_f\right|, & \dot{x}_f\left(\dot{x}_f - \dot{w}_f\right) \geq 0 \\ 0, & \dot{x}_f\left(\dot{x}_f - \dot{w}_f\right) < 0 \end{cases} \tag{3.3}$$

where i_{f0} and i_{r0} are constants.

As it was mentioned previously, algorithms CA2 and CA3 require that an inverse model of a damper is applied. An inverse model, based on the Spencer model, lacks the required accuracy as the input currents are ascribed to damper force and piston velocity values in an ambiguous manner, due to the presence of a hysteresis. Current profiles reveal step fluctuations even under minor continuous variations of force or piston velocity. In the light of the above considerations, the inverse model was developed omitting the hysteresis [3, 16].

An inverse model is represented as the mapping procedure ascribing input currents to damper force and piston velocity values. This mapping is based on measurement data obtained during the testing of the RD-1005-3 damper. Measurements of the damper force were taken under triangular base excitations with the amplitude 3.8×10^{-3} m and frequencies: 0.33, 0.67, 1.00, 1.33, 1.67, 2.00, 2.50, 3.00, 4.00, 5.33, 6.67, 8.00 Hz. Measurements were performed for the input current levels: 0.00, 0.02, 0.04, 0.06, 0.08, 0.10, 0.12, 0.14, 0.16, 0.18, 0.20, 0.25, 0.30, 0.40, 0.60, 0.80 A. From the discretised mapping of the damper force, piston velocity and input current, this portion is used in which force would vary in the range (–600, +600) N, the corresponding input current level is (0.00, 0.20) A. This limit was adopted on the basis of theoretical and experimental data.

Figure 2 shows a schematic diagram of a cascade controller utilizing an algorithm CA2.

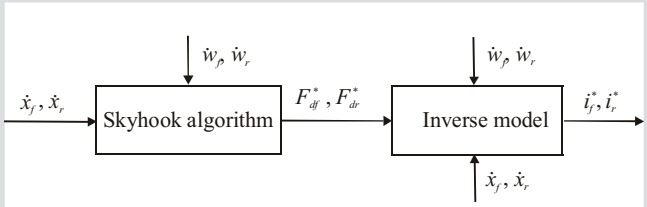

Fig. 2. Diagram of CA2 algorithm (skyhook in conjunction with inverse model)

Two blocks are apparent on this diagram. The inputs to the first block are velocities: $\dot{x}_f, \dot{x}_r, \dot{w}_f$ and $\dot{w}_r$, determined through the measurement of displacements: x_f, x_r, w_f and w_r, and their differentiation. The outputs are optimal values of the dampers' forces according to the skyhook concept. Forces F_{df}^* and F_{dr}^* are derived from equations (3.1) and (3.2).

In the other block the inverse model is implemented – force and piston velocity values are utilized to find reference input currents i_f^* and i_r^*.

The CA3 utilizes an LQ control algorithm. LQ control is the stabilizing strategy applicable to linear dynamic systems. It is the optimal control in the aspect of the adopted performance index.

The dynamics of a plant to be controlled is governed by equation (2.11). The state vector $\boldsymbol{X}$ and the input vector $\boldsymbol{U}$ are the real variables of time, whilst the matrices $\boldsymbol{A}$ and $\boldsymbol{B}$ are constant real matrices. A linear-quadratic control theory with continuous time was recalled to formulate the control problem. This approach can be justified by the fact that sampling frequency assumed in experiments is large while compared to frequency of damper vibration of the considered system and frequency of harmonic excitations.

The state of the system $\boldsymbol{X} = \left[x \quad \dot{x} \quad \varphi \quad \dot{\varphi}\right]^{\mathrm{T}}$ is available during experiments on the basis of: x_f, x_r, $\dot{x}_f$ and $\dot{x}_r$. For a system governed by equation (2.11) the LQ control problem is formulated in a general way – with the finite time horizon $\tau \in [0,\ t_f)$ [4]. The performance index for this problem is written as:

$$\boldsymbol{J}_{LQ}(t_f) = \int_0^{t_f} \Big\{ \left[\boldsymbol{X}(\tau)\right]^{\mathrm{T}} \boldsymbol{Q}\boldsymbol{X}(\tau) + \left[\boldsymbol{U}(\tau)\right]^{\mathrm{T}} \boldsymbol{R}\boldsymbol{U}(\tau) + \ldots$$
$$\ldots + 2\left[\boldsymbol{X}(\tau)\right]^{\mathrm{T}} \boldsymbol{N}\boldsymbol{U}(\tau) + \left[\boldsymbol{X}(t_f)\right]^{\mathrm{T}} \boldsymbol{D}_f \boldsymbol{X}(t_f) \Big\} d\tau \tag{3.4}$$

where $\boldsymbol{Q}$, $\boldsymbol{R}$, $\boldsymbol{N}$, $\boldsymbol{D}_f$ are constant matrices of coefficients that fulfill the following conditions:

$$\boldsymbol{\Pi} = \begin{bmatrix} \boldsymbol{Q} & \boldsymbol{N} \\ \boldsymbol{N}^{\mathrm{T}} & \boldsymbol{R} \end{bmatrix} = \boldsymbol{\Pi}^{\mathrm{T}} \geq \boldsymbol{0}, \quad \boldsymbol{R} > \boldsymbol{0}.$$

Desired values of state vector elements $\boldsymbol{X}(t_f)$ are all equal to zero.

It is well known that if a pair ($\boldsymbol{A}$, $\boldsymbol{B}$) is stabilisable and a pair ($\boldsymbol{A}$, $\boldsymbol{Q}$) is detectable, there is precisely one control input $\boldsymbol{U}^* \in \mathsf{U}$, $\mathsf{U}=\{\boldsymbol{U} \in \mathsf{L}^2([0, t_f],\mathsf{R}^n)$: $\boldsymbol{J}_{LQ}(U)<+\infty\}$ such that

$$\underset{\boldsymbol{U}\in\mathsf{U}}{\forall} J_{LQ}\left(\boldsymbol{U}^*\right) \leq J_{LQ}\left(\boldsymbol{U}\right)$$

while

$$\boldsymbol{U}^* = -\boldsymbol{K}^*(\tau)\boldsymbol{X}^*, \boldsymbol{K}^*(\tau) = \boldsymbol{R}^{-1}[\boldsymbol{N}^{\mathrm{T}} + \boldsymbol{B}^{\mathrm{T}}\boldsymbol{D}(\tau)] \tag{3.5}$$

where $\boldsymbol{D}(\tau) = [\boldsymbol{D}(\tau)]^T \geq \boldsymbol{0}$ is the only solution to the Riccati differential equation

$$\begin{aligned} &\boldsymbol{A}^{\mathrm{T}}\boldsymbol{D}(\tau) + \boldsymbol{D}(\tau)\boldsymbol{A} - \\ &-[\boldsymbol{D}(\tau)\boldsymbol{B} + \boldsymbol{N}]\boldsymbol{R}^{-1}[\boldsymbol{B}^{\mathrm{T}}\boldsymbol{D}(\tau) + \boldsymbol{N}^{\mathrm{T}}] + \boldsymbol{Q} = -\dot{\boldsymbol{D}}(\tau) \\ &\boldsymbol{D}_f = \boldsymbol{D}(t_f) \end{aligned} \tag{3.6}$$

and $\boldsymbol{X}^*$ is the optimal trajectory of state, fulfilling the feedback system equation

$$\dot{\boldsymbol{X}}^* = [\boldsymbol{A} - \boldsymbol{B}\boldsymbol{K}^*(\tau)]\boldsymbol{X}^* \tag{3.7}$$

The optimal value of the performance index is given as

$$\boldsymbol{J}^*_{LQ}(t_f) = (\boldsymbol{X}_0)^{\mathrm{T}}\boldsymbol{D}(0)\boldsymbol{X}_0 \tag{3.8}$$

The LQ control algorithm was applied to the suspension system [8, 9, 15] assuming that the quantities F_{df} and F_{dr} described by nonlinear relationships are elements of vector $\boldsymbol{U}$ (2.11). Due to the complexity of the computation procedure and the risk of bad conditioning of the problem written in the form of equations (3.4)–(3.6) in each subsequent sampling cycle, a boundary case of LQ control is considered with an infinite time horizon. In the case when control time is finite, the solution to LQ problem with infinite time horizon governed by equation (3.10) is only an approximation of optimal control (3.5). However, the procedure to obtain the solution written as equation (3.10) is less sensitive to errors associated with incorrect matrix conditioning. For $t_f \to \infty$, the performance index $J_{LQ}(t)$ given by equation (3.4) is rewritten as

$$\begin{aligned} J_{LQ} = \int_0^\infty \Big\{ &[\boldsymbol{X}(\tau)]^{\mathrm{T}}\boldsymbol{Q}\boldsymbol{X}(\tau) + [\boldsymbol{U}(\tau)]^{\mathrm{T}}\boldsymbol{R}\boldsymbol{U}(\tau) + \\ &+2[\boldsymbol{X}(\tau)]^{\mathrm{T}}\boldsymbol{N}\boldsymbol{U}(\tau)\Big\} d\tau \end{aligned} \tag{3.9}$$

where: $\boldsymbol{\Pi} = \begin{bmatrix} \boldsymbol{Q} & \boldsymbol{N} \\ \boldsymbol{N}^{\mathrm{T}} & \boldsymbol{R} \end{bmatrix} = \boldsymbol{\Pi}^{\mathrm{T}} \geq \boldsymbol{0}, \quad \boldsymbol{R} > \boldsymbol{0}.$

Similarly to the general case, if a pair ($\boldsymbol{A}$, $\boldsymbol{B}$) is stabilisable and pair ($\boldsymbol{A}$, $\boldsymbol{Q}$) detectable, there exists precisely one control input: $\boldsymbol{U}^* \in \mathsf{U}$, $\mathsf{U}=\{\boldsymbol{U} \in \mathsf{L}^2([0, \infty],\mathsf{R}^n)$: $\boldsymbol{J}_{LQ}(U)<+\infty\}$, that is optimal for $t_f \to \infty$, so that

$$\boldsymbol{U}^* = -\boldsymbol{K}^*\boldsymbol{X}^*, \boldsymbol{K}^* = \boldsymbol{R}^{-1}[\boldsymbol{N}^{\mathrm{T}} + \boldsymbol{B}^{\mathrm{T}}\boldsymbol{D}] \tag{3.10}$$

where the constant matrix $\boldsymbol{D} = \boldsymbol{D}^T \geq \boldsymbol{0}$ is the only solution to an algebraic Riccatti equation

$$\boldsymbol{A}^{\mathrm{T}}\boldsymbol{D} + \boldsymbol{D}\boldsymbol{A} - [\boldsymbol{D}\boldsymbol{B} + \boldsymbol{N}]\boldsymbol{R}^{-1}[\boldsymbol{B}^{\mathrm{T}}\boldsymbol{D} + \boldsymbol{N}^{\mathrm{T}}] + \boldsymbol{Q} = \boldsymbol{0} \tag{3.11}$$

and $\boldsymbol{X}^*$ is the optimal trajectory of state, fulfilling the conditions of the feedback system

$$\dot{\boldsymbol{X}}^* = (\boldsymbol{A} - \boldsymbol{B}\boldsymbol{K}^*)\boldsymbol{X}^* \tag{3.12}$$

Accordingly, the optimal value of the performance index is

$$J^*_{LQ} = (\boldsymbol{X}_0)^{\mathrm{T}}\boldsymbol{D}\boldsymbol{X}_0 \tag{3.13}$$

Basing on the considered LQ control problem, a cascade algorithm CA3 is proposed for the control of MR dampers. This algorithm is tuned with an eye to minimize accelerations.

Figure 3 shows a schematic diagram of a cascade controller in conjunction with an algorithm CA3 [6, 13]. Two blocks are readily apparent on the diagram. The inputs to the first block are: bounce and angular displacements and velocities of the system cog and excitations w_f, w_r. The outputs are optimal values of the damper forces according to the LQ concept. The second block implements the inverse model of the damper.

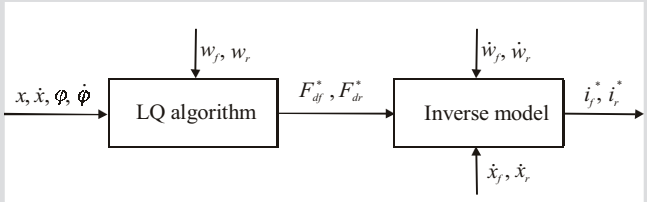

Fig. 3. Diagram of CA3 algorithm
(LQ algorithm in conjunction with inverse model)

In the first block the reference values of the damper forces (F^*_{df} and F^*_{dr}), which minimize the adopted performance index J_{LQ}, are determined. The solution (3.10) obtained for the system governed by equation (2.11) becomes the output of the cascade controller's first block utilizing the CA3 algorithm.

An inverse model of the damper in the front (rear) section for an instantaneous piston velocity $\dot{x}_f - \dot{w}_f$ ($\dot{x}_r - \dot{w}_r$) determines the value of the input current $i^*_f(i^*_r)$ which corresponds to the damper force $F^*_{df}(F^*_{dr})$ derived in the first block.

Let us proceed to the description of the synthesis of an LQ algorithm. The performance index for the suspension system is written as

$$J_{LQ} = \int_0^\infty \Big\{ q_x \left[x(\tau)\right]^2 + q_\varphi \left[\varphi(\tau)\right]^2 + q_{\dot{x}} \left[\dot{x}(\tau)\right]^2 + q_{\dot{\varphi}} \left[\dot{\varphi}(\tau)\right]^2 + q_{\ddot{x}} \left[\ddot{x}(\tau)\right]^2 + q_{\ddot{\varphi}} \left[\ddot{\varphi}(\tau)\right]^2 + r_{\mathbf{U}f} \left[F_{df}(\tau)\right]^2 + \\ + r_{\mathbf{U}r} \left[F_{dr}(\tau)\right]^2 + 2 r_{\mathbf{U}f} k F_{df}(\tau) w_f(\tau) + 2 r_{\mathbf{U}r} k F_{dr}(\tau) w_r(\tau) + r_{\mathbf{U}f} \left[k w_f(\tau)\right]^2 + r_{\mathbf{U}r} \left[k w_r(\tau)\right]^2 \Big\} d\tau \tag{3.14}$$

where:

$q_x, q_\varphi, q_{\dot{x}}, q_{\dot{\varphi}}, q_{\ddot{x}}, q_{\ddot{\varphi}}$ – weighting factors corresponding to variables x, φ, $\dot{x}$, $\dot{\varphi}$, $\ddot{x}$, $\ddot{\varphi}$;

r_{Uf}, r_{Ur} – weighting factors corresponding to first (front) and second (rear) element of input vector $\boldsymbol{U}$ (2.14).

Substituting equations (2.9) and (2.10) into equation (3.14) yields the performance index J_{LQ} in a matrix form

$$\boldsymbol{J}_{LQ} = \int_0^\infty \Big\{ \left[\boldsymbol{X}(\tau)\right]^{\mathrm{T}} \boldsymbol{Q} \boldsymbol{X}(\tau) + \left[\boldsymbol{U}(\tau)\right]^{\mathrm{T}} \boldsymbol{R} \boldsymbol{U}(\tau) + 2 \left[\boldsymbol{X}(\tau)\right]^{\mathrm{T}} \boldsymbol{N} \boldsymbol{U}(\tau) \Big\} d\tau \tag{3.15}$$

where:

$$\boldsymbol{Q} = \begin{bmatrix} q_x + \dfrac{4k^2}{m^2} q_{\dot{x}} + \dfrac{k^2 \left(l_f - l_r\right)^2}{J^2} q_{\ddot{\varphi}} & 0 & \dfrac{2k^2 \left(l_f - l_r\right)}{m^2} q_{\dot{x}} + \dfrac{k^2 \left(l_f - l_r\right)\left(l_f^2 + l_r^2\right)}{J^2} q_{\ddot{\varphi}} & 0 \\ 0 & q_{\dot{x}} & 0 & 0 \\ \dfrac{2k^2 \left(l_f - l_r\right)}{m^2} q_{\dot{x}} + \dfrac{k^2 \left(l_f - l_r\right)\left(l_f^2 + l_r^2\right)}{J^2} q_{\ddot{\varphi}} & 0 & \dfrac{k^2 \left(l_f - l_r\right)^2}{m^2} q_{\dot{x}} + q_\varphi + \dfrac{k^2 \left(l_f^2 + l_r^2\right)^2}{J^2} q_{\ddot{\varphi}} & 0 \\ 0 & 0 & 0 & q_{\dot{\varphi}} \end{bmatrix},$$

$$\boldsymbol{R} = \begin{bmatrix} r_{\mathbf{U}_f} + \dfrac{1}{m^2} q_{\ddot{x}} + \dfrac{l_f^2}{J^2} q_{\ddot{\varphi}} & \dfrac{1}{m^2} q_{\ddot{x}} - \dfrac{l_f l_r}{J^2} q_{\ddot{\varphi}} \\ \dfrac{1}{m^2} q_{\ddot{x}} - \dfrac{l_f l_r}{J^2} q_{\ddot{\varphi}} & r_{\mathbf{U}_r} + \dfrac{1}{m^2} q_{\ddot{x}} + \dfrac{l_r^2}{J^2} q_{\ddot{\varphi}} \end{bmatrix},$$

$$\boldsymbol{N} = \begin{bmatrix} -\dfrac{2k}{m^2} q_{\ddot{x}} - \dfrac{k l_f \left(l_f - l_r\right)}{J^2} q_{\ddot{\varphi}} & -\dfrac{2k}{m^2} q_{\dot{x}} + \dfrac{k l_r \left(l_f - l_r\right)}{J^2} q_{\ddot{\varphi}} \\ 0 & 0 \\ -\dfrac{k \left(l_f - l_r\right)}{m^2} q_{\ddot{x}} - \dfrac{k l_f \left(l_f^2 + l_r^2\right)}{J^2} q_{\ddot{\varphi}} & -\dfrac{k \left(l_f - l_r\right)}{m^2} q_{\dot{x}} + \dfrac{k l_r \left(l_f^2 + l_r^2\right)}{J^2} q_{\ddot{\varphi}} \\ 0 & 0 \end{bmatrix}.$$

As the vertical and angular acceleration acting upon the beam cog serve as the basic criteria of suspension vibration isolation quality, the weighing factors values for accelerations are assumed to be: $q_{\ddot{x}} = 6.31 \times 10^4$, $q_{\ddot{\varphi}} = 6.31 \times 10^4$, while for displacements: q_x =1 and q_φ=1. In order to increase the forces F_{df} and F_{dr} at resonant frequencies, the weighing factors values for velocities are $q_{\dot{x}} = 2 \times 10^8$ and $q_{\dot{\varphi}} = 2 \times 10^8$. The values: $r_{Uf} = r_{Ur} = 1.58 \times 10^{-3}$ are taken to be relatively small on account of a large force margins of MR dampers. It is apparent that base excitations w_f and w_r are not subject to control (though they are incorporated in the vector $\boldsymbol{U}$) thus their influence on r_{Uf} and r_{Ur} is not considered. The performance index components associated with w_f and w_r are neglected while assessing the quality of vibration isolation.

For experimental model parameter values and for weighing factors specified above, all sufficient and necessary conditions are fulfilled for there being precisely one control $\boldsymbol{U}^* = -\boldsymbol{K}^*\boldsymbol{X}$ (optimal one in the context of equations (3.14) and (3.15) provided that $\boldsymbol{X} = \boldsymbol{X}^*$): the pair $(\boldsymbol{A}, \boldsymbol{B})$ is stabilisable and pair $(\boldsymbol{A}, \boldsymbol{Q})$ detectable and $\boldsymbol{\Pi} = \boldsymbol{\Pi}^T > 0, \boldsymbol{R} > 0$. The solution to the LQ problem is obtained in the form

$$\boldsymbol{U}^* = \begin{bmatrix} F_{df}^* + kw_f \\ F_{dr}^* + kw_r \end{bmatrix} = -\boldsymbol{K}^* \begin{bmatrix} x \\ \dot{x} \\ \varphi \\ \dot{\varphi} \end{bmatrix}, \tag{3.16}$$

$$\text{thus} \qquad \begin{bmatrix} F_{df}^* \\ F_{dr}^* \end{bmatrix} = -\boldsymbol{K}^* \begin{bmatrix} x \\ \dot{x} \\ \varphi \\ \dot{\varphi} \end{bmatrix} - k \begin{bmatrix} w_f \\ w_r \end{bmatrix}$$

where:

$$\boldsymbol{K}^* = \begin{bmatrix} -4.082 & 0.715 & -2.918 & 0.198 \\ -4.082 & 0.715 & 2.918 & -0.198 \end{bmatrix} \times 10^4 \tag{3.17}$$

Outputs from the first block of the algorithm CA3: F_{df}^* and F_{dr}^* are the inputs of the inverse model; its outputs are reference currents i_f^*, i_r^* at which (for the appropriate velocities $\dot{x}_f - \dot{w}_f, \dot{x}_r - \dot{w}_r$ senses) the damper forces are equal to F_{df}^*, F_{dr}^*. It has to be emphasized that designations i_f^* and i_r^* are arbitrary (stars indicate reference values, not the optimal ones) as precise mapping of resistance forces F_{df}^* and F_{dr}^* (optimal for $t \to \infty$) determined in the first block of algorithm CA3 is not possible when controllable dampers are used. Therefore, the trajectory $\boldsymbol{X}$ is only an approximation of $\boldsymbol{X}^*$ ($\boldsymbol{X} \neq \boldsymbol{X}^*$) and hence the components F_{df}^* and F_{dr}^* of the vector $\boldsymbol{U}^*$ shall also be treated as reference, not optimal ones.

For the considered control algorithms CA1, CA2, CA3, upper limits of input currents are introduced: $i_f \le i_{fm}$, $i_r \le i_{rm}$. The limit value $i_{fm} = i_{rm} = i_m$ is taken depending on the operating characteristics of feedback systems. In the consequence, effective *rms* values of input currents are reduced, and so are acceleretions: $\ddot{x}, \ddot{\varphi}$ and jerks: $\dddot{x}, \dddot{\varphi}$ values above the resonance frequency band. That did not cause any major deterioration of vibration damping at resonance frequency, which effect was evident when the CA3 algorithm was applied and the control values were restricted (i.e. when the values of weighing factors r_{Uf} and r_{Ur} were increased).

4. PERFORMANCE INDICES

The vibration isolation performance of a system with open loop and feedback CA1, CA2, CA3 structures was compared by introducing the transmissibility factors denoted by: T_x, T_φ, $T_{\ddot{x}}^{rms}$ and $T_{\ddot{\varphi}}^{rms}$. These factors are defined by equations (4.1)–(4.4).

The factor T_x is the quotient of amplitude A_x of vertical displacement of beam's cog x and the amplitude A_{wx} of the mean value of vertical excitation $w_x = (w_f + w_r)/2$

$$T_x = \frac{A_x}{A_{wx}} \tag{4.1}$$

The factor T_φ is the quotient of the amplitude A_φ of beam pitch displacement (with respect to its cog) φ and the amplitude $A_{\omega\varphi}$ of the mean angular excitation $w_\varphi = (w_f - w_r)/(l_f + l_r)$.

$$T_\varphi = \frac{A_\varphi}{A_{w\varphi}} \tag{4.2}$$

The factor $T_{\ddot{x}}^{rms}$ is the quotient of root-mean-square (*rms*) value of the vertical acceleration of the beam cog $rms(\ddot{x})$, and the *rms* value of the second order derivative of the mean vertical excitation $rms(\ddot{w}_x)$

$$T_{\ddot{x}}^{rms} = \frac{rms(\ddot{x})}{rms(\ddot{w}_x)} \tag{4.3}$$

$T_{\ddot{\varphi}}^{rms}$ is the quotient of the *rms* value of the angular acceleration of the beam with respect to its cog $rms(\ddot{\varphi})$ and *rms* value of the second order derivative of the mean angular excitation $rms(\ddot{w}_\phi)$

$$T_{\ddot{\varphi}}^{rms} = \frac{rms(\ddot{\varphi})}{rms(\ddot{w}_\varphi)} \tag{4.4}$$

5. EXPERIMENTAL SETUP

As the investigations were limited to pitch-plane oscillations, the experimental setup conformed to the appropriate construction demands, namely transverse rigidity. All the motion components orthogonal to the pitch-plane, or other than pitch and bounce, were eliminated. This implied the use of appropriate central guiding elements with adequately small friction forces. All the joints had high transverse rigidity. Limited output of the available shakers implied constraints to the total mass and moment of inertia of the sprung system.

The diagram of the experimental setup with a pitch-plane model of a vehicle suspension system is shown in Figure 4.

The measurement and control system was based on a PC with RT-DAC4 multi I/O board installed. The system was supported by MATLAB/Simulink 7.0 and RTW/RTWT running on Windows XP.

The experiments were conducted by means of four linear voltage displacement transducers (LVDT), two of them located on the beam – displacements x_f and x_r, and the other two on the shakers – displacements w_f and w_r, and RT-DAC4 multi I/O board installed in a PC. Based on the measured displacements x_f and x_r we obtained vertical displacement x and pitch displacement φ of beam's cog. The velocities were reproduced using derivative blocks of Simulink.

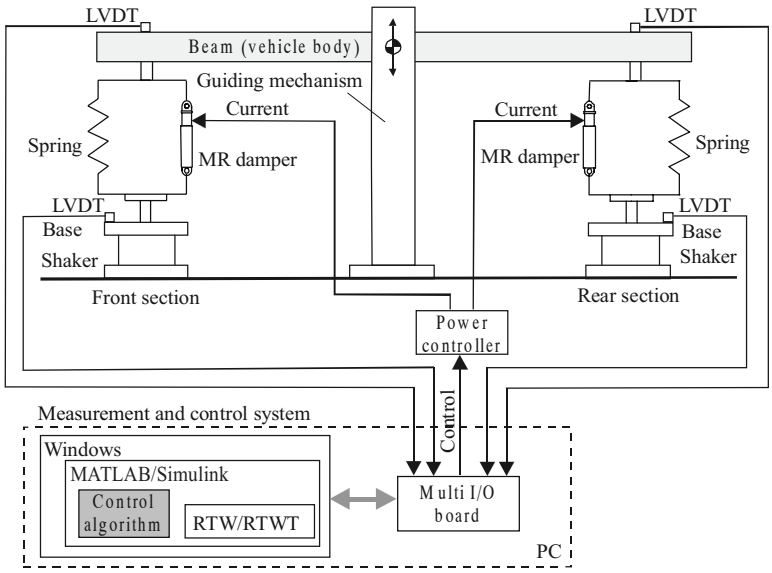

Fig. 4. Diagram of the experimental setup

The input currents i_f^* and i_r^* calculated in MATLAB/Simulink were output by means of RTWT/RTW and RT-DAC4, then converted to the signals of multi-channel power controller and applied to the dampers.

The photograph of the system ready for tests is presented in Figure 5. Experimental setup comprised: steel beam as a load element (vehicle body), two identical suspension-sets: specially designed spring and RD 1005-3 damper, central roller guiding and two shakers. Each suspension-set was built as a parallel connection of a vertically mounted damper inside and outer screw-cylindrical reflex spring guided onto two thin-wall sleeves. The sleeves were guided one inside the other with teflon slide ring between them. Both sleeves possess outer flanges as the spring support. A suspension-set was connected at the top with the beam and at the bottom with the shaker by means of pin joints.

The beam's cog was connected by means of pin joints to the car elements moving inside vertically mounted guiding rails utilizing roller bearing. This guaranteed longitudinal and transversal rigidity of the system. The guiding rails and shaker were mounted on the rigid cubicoid steel frame. This suspension design ensures that the investigated system possesses two degrees of freedom.

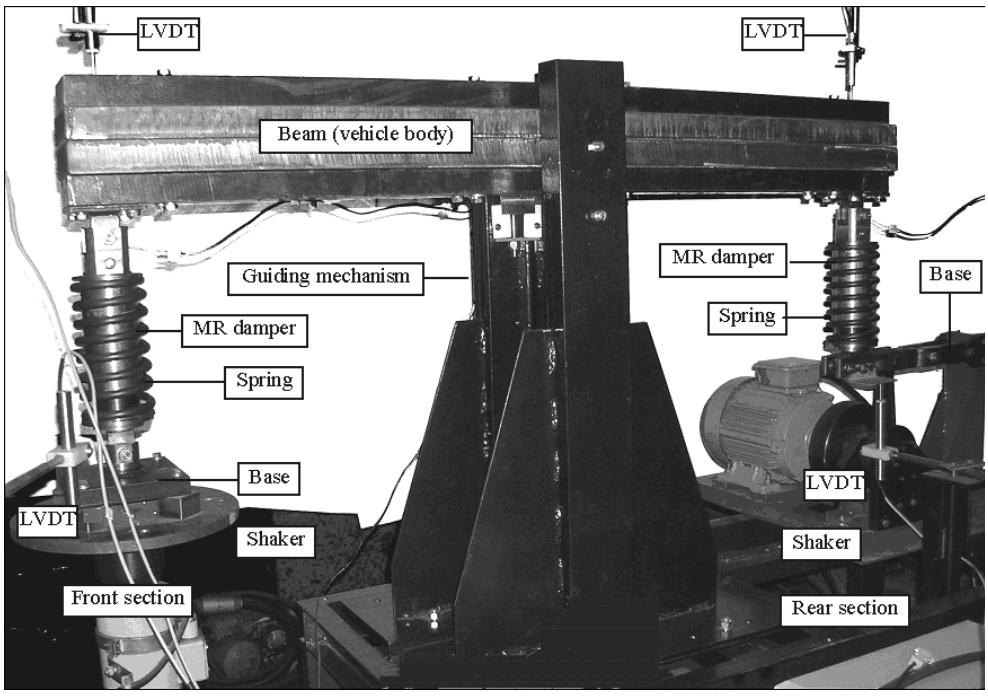

Fig. 5. Photograph of the pitch-plane model of a vehicle suspension ready for tests

Two shakers were available in experiments. One of them was an electro-hydraulic shaker that was computer controlled. The other shaker (AC motor supplied by the electronic inverter with circular cam crank mechanism) enabled us smooth control of rotation speed and excitation frequency in the range of (2, 10) Hz [7].

6. EXPERIMENTS

We applied double-sided base-excitations w_f, w_r and one-sided base-excitation w_f (then $w_r = 0$) for the suspension system. The double-sided excitations were sine waves with either the same frequency, amplitude and phase ($w_f = w_r$) or with the same frequency and phase but opposite amplitudes ($w_f = -w_r$). The first ones were vertical displacement excitations of the beam. Such excitations act on a vehicle traveling over long and middle-sized longitudinal ground unevenness. The second type of excitations was longitudinal (or lateral) pitching. Due to nonlinearity of MR damper characteristics, a coupling effect occurs and vertical vibrations are induced, too [6]. Such excitations act upon a vehicle traveling over short longitudinal obstacles on the ground and upon the vehicle body during fast manoeuvres: veering, braking, and accelerating. In both cases the frequency of excitations was varied in the range (2, 10) Hz and the amplitude was set to be 3.8×10^{-3} m.

The one-sided, square excitations w_f ($w_r = 0$) induced the coupled beam vibrations (combining vertical and pitch vibrations). Such excitations are encountered when a vehicle rides over an obstacle on the ground with steep, vertical edges.

Investigation of feedback system enabled us to check the adequacy of the operating principle of the CA1, CA2 and CA3 algorithms for MR dampers control. The input currents applied for all algorithms were assumed to be equal to the reference input currents i_f^* and i_r^*. The constants of CA1, CA2 and CA3 algorithms were established numerically and verified experimentally:

CA1: $i_{f0} = i_{r0} = 2$ A·s/m, $i_m = 0.15$ A;

CA2: $c_{sky} = 3000$ N·s/m, $i_m = 0.15$ A;

CA3: $\boldsymbol{K}$ defined by equation (3.17), $i_m = 0.20$ A.

Experiments were conducted with the sampling frequency of 1 kHz.

In the first stage we determined frequency responses of an open loop system under double-sided excitations $w_f = w_r$ when the input currents were either 0.00 A or 0.20 A. Similarly we received frequency responses of feedback system by applying CA1, CA2 and CA3 algorithms.

Selected plots are presented in Figures 6–9. The plots indicate vertical and angular displacement transmissibilities T_x, T_φ, and vertical and angular *rms* acceleration transmissibilities $T_{\ddot{x}}^{rms}$, $T_{\ddot{\varphi}}^{rms}$ achieved for open loop and feedback systems.

Figures 6–9 indicate that the resonance frequencies of the suspension system equipped with MR dampers at 0.00 A lie within the ranges: $f_x \in (2.7, 3.0)$ Hz (bounce) and $f_\varphi \in (4.0, 4.5)$ Hz (pitch), and they increase with the increase of MR dampers' input currents. The accuracy in

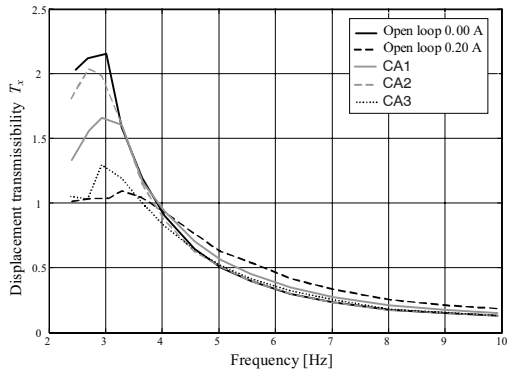

Fig. 6. Displacement transmissibility T_x

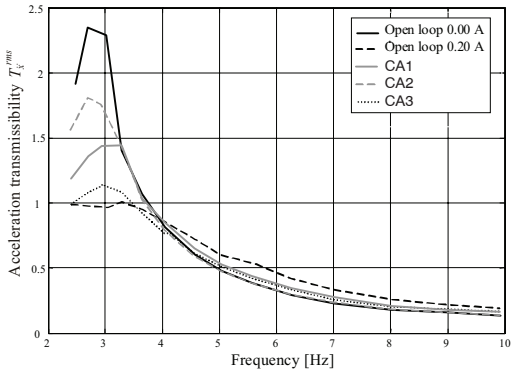

Fig. 7. Acceleration transmissibility $T_{\ddot{x}}^{rms}$

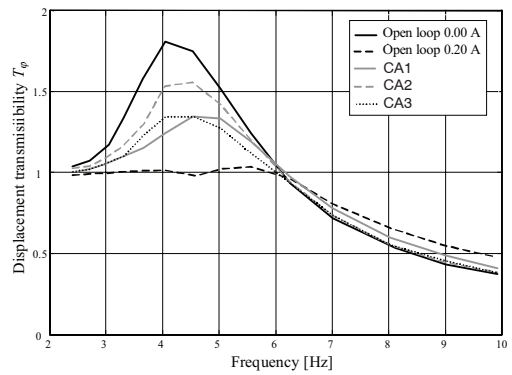

Fig. 8. Displacement transmissibility T_φ

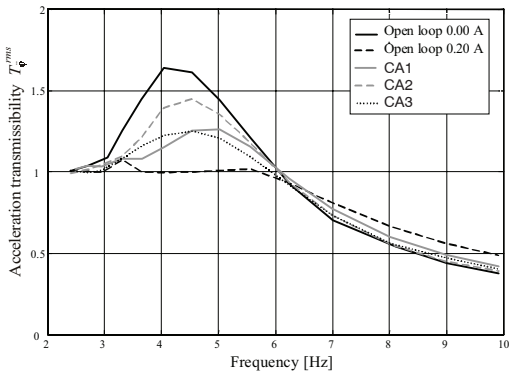

Fig. 9. Acceleration transmissibility $T_{\ddot{\varphi}}^{rms}$

determining the resonance frequencies f_x and f_φ was limited by the adopted frequency step of the analyzed excitation frequencies. It is apparent that as the input current was increased to 0.20 A, the resonance peak was attenuated but isolation was lost at higher frequencies. This was due to MR damper behaviour.

In comparison with the open loop system at input current level 0.00 A, all the feedback systems CA1, CA2, CA3 provided vibration reduction in the resonance frequency range both in terms of vertical motion and longitudinal pitching. The range of input currents was established through simulations to be (0.00, 0.20) A, which enabled us to effectively control resonant frequencies of the suspension model.

Experimental data reveals that feedback system in conjunction with CA3 algorithm (utilizing the solution of the LQ control problem and the inverse model of the MR damper) ensures the most favourable properties in terms of minimisation of accelerations in the most sensitive for human range of (4, 10) Hz. It should be noted that the applied for CA3 secondary signal-smoothing (in place of the input filters used for CA1 and CA2) vastly improved the vibration isolation performance of the system at low excitation frequencies (including resonance). However, a slight increase of the transmissibility factors: T_x, $T_{\ddot{x}}^{rms}$, T_φ and $T_{\ddot{\varphi}}^{rms}$ for super-resonance frequencies is observed (while compared to the values obtained for the open loop system at 0.00 A).

At super-resonance frequencies algorithms CA2 and CA3 ensure the best performance – the transmissibility ratios $T_{\ddot{x}}^{rms}$ and $T_{\ddot{\varphi}}^{rms}$ are approximately equal to those of the open loop system at 0.00 A. For the feedback system with algorithm CA1, values of transmissibility factors describing vertical vibrations (T_x and $T_{\ddot{x}}^{rms}$) were significantly increased at excitation frequencies higher than 3.5 Hz; similarly the values of factors: T_φ and $T_{\ddot{\varphi}}^{rms}$ above 6 Hz [10]. However, the algorithm CA1 is more efficient than CA2 in reduction of resonance vibrations.

Figure 10 shows displacement x_f (in reference to x_f for the open loop system at 0.00 A and excitation w_f) and reference input current i_f^* profiles obtained by applying CA1, CA2 and CA3 algorithms under doubled-sided sine base excitation $w_f = w_r$ with frequency $f = 3.01$ Hz (hence in the resonance range of the vertical motion). When analyzing the plots, attention must be given to the reduction of amplitude and phase lag of displacement x_f in the feedback system when compared to an open loop system at 0.00 A. Note that the input current i_f^* is nonzero when $|\dot{w}_f| < |\dot{x}_f|$, hence increasing the damper force at those time instants causes the displacement and acceleration amplitudes (x_f and $\ddot{x}_f$) to decrease. Furthermore, the input current i_f^* equals zero when the signs of the velocities $\dot{x}_f - \dot{w}_f$ and $\dot{x}_f$ are opposite. When the algorithm CA3 is applied, the displacement amplitude x_f is reduced more significantly than for feedback system with CA1 and CA2 (Fig. 10).

Next we measured time responses of an open loop system under one-sided square base excitation with amplitude of 3.8×10^{-3} m for various input currents applied to the dampers. Figure 11 shows selected plots obtained for input currents of 0.00 A and 0.20 A. The plots reveal that x_f overshoot amplitude decreased as the input current increased.

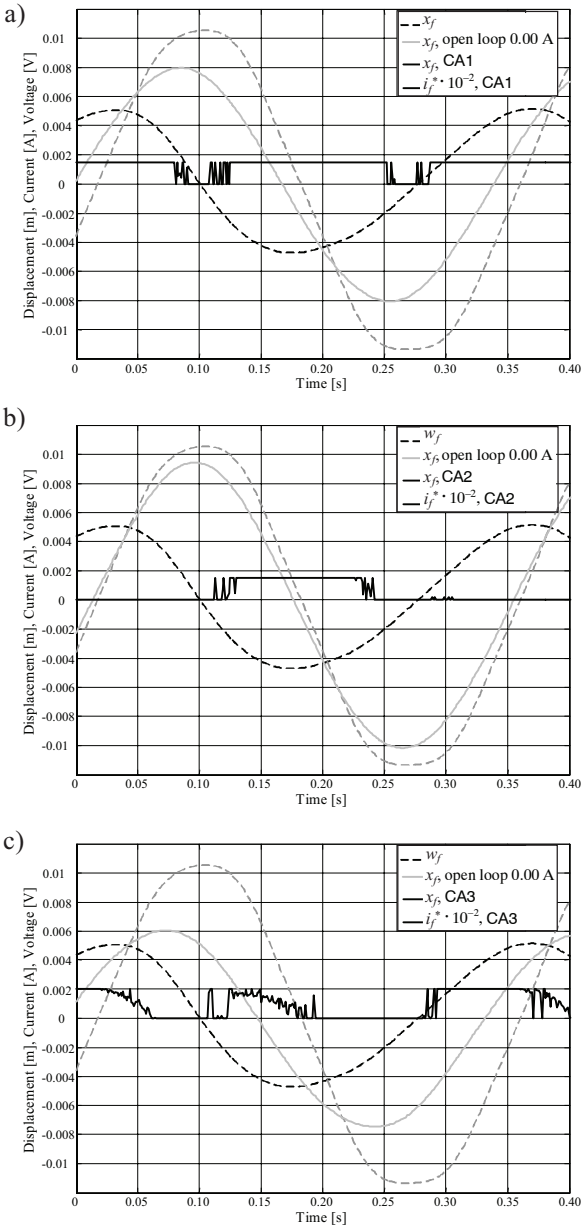

Fig. 10. Double-sided sine base excitation $w_f = w_r$ with frequency 3.01 Hz, displacement x_f, and input current i_f^* for feedback systems CA1 (a), CA2 (b) and CA3 (c), in comparison with open loop system at 0.00 A

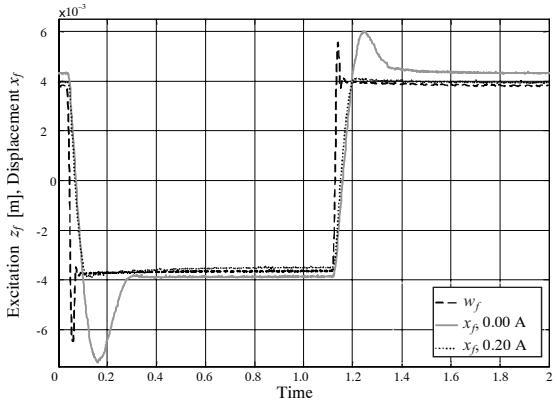

Fig. 11. One-sided square base excitation w_f, displacement x_f for open loop systems

Figure 12 shows displacement x_f and reference input current i_f^* obtained by applying algorithms CA1, CA2 and CA3 under one-sided square base excitations w_f. Measurement data for the feedback systems lead us to the following conclusions.

The input current reduces the overshoot apparent for the open loop system at 0.00 A. Besides, the numerous switches of the input current i_f^* between the maximal value and the minimal one (i.e. zero) can be observed in the time intervals (0.3, 1) s after the excitation edge.

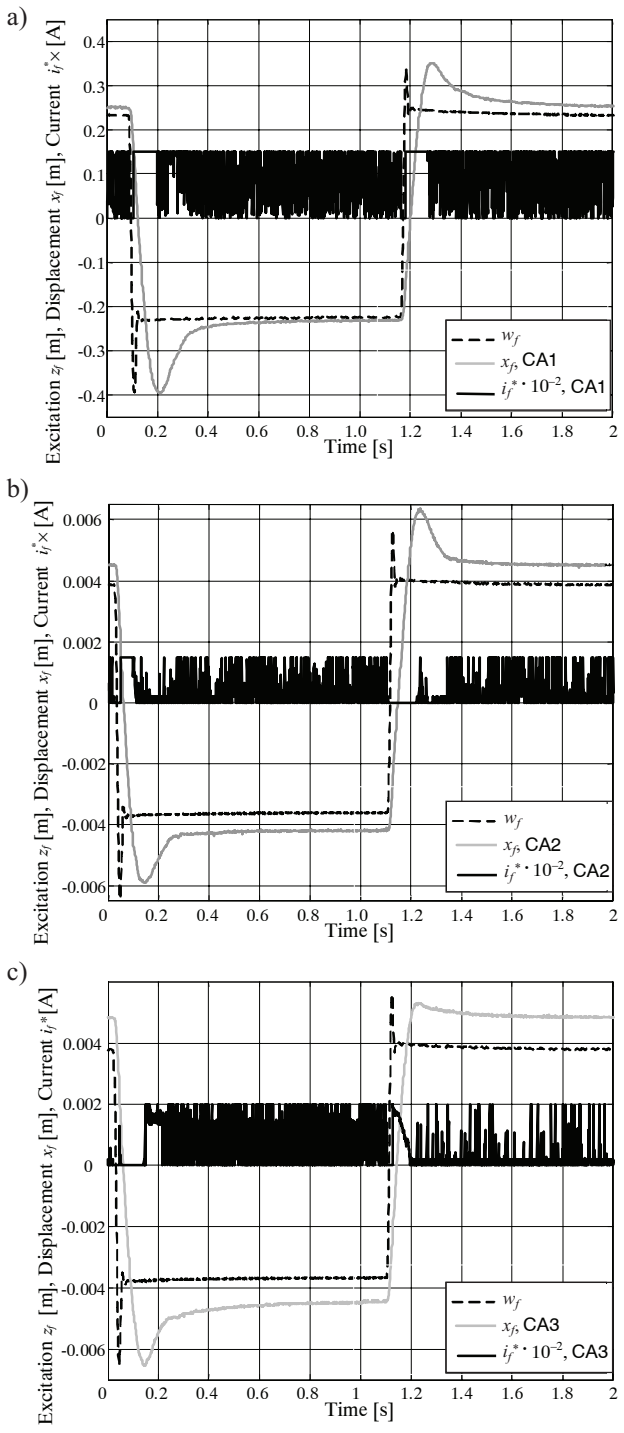

Fig. 12. One-sided square base excitation w_f, displacement x_f, and input current i_f^* for feedback systems CA1 (a), CA2 (b) and CA3 (c)

That is caused by the delayed damper response to input current variations and the enhanced system response to the nonzero value of $\dot{x}_f$, associated with slow reaching of the static deflection point of the damper and spring in front section during the relevant time intervals. In order to minimise $|\dot{x}_f|$, the maximal admissible input current (since $\dot{w}_f = 0$) was set. The asso-ciated increase of force F_{df} caused the piston velocity $|\dot{x}_f|$ to fall to zero; the elimination of the control error resulted in turn in input current reduction to zero, whilst $|\dot{x}_f|$ was increasing. Such a cycle repeated numerous times.

Of particular interest is the difference in nature of the currents i_f^* in the feedback system for each applied control algorithm CA1, CA2 and CA3. In the case of CA3, input current reaches higher values for the ascending edge of the applied excitation w_f (in order to minimize the overshooting). For the descending edge, this current has nonzero value only for 5×10^{-3} s.

In the case of CA2, input current assumes nonzero value for the negative (descending) edge of the excitation w_f. When the edge is positive (ascending) the input current equals zero. This phenomenon can be explained as follows. In an open-loop system at 0.00 A the descending edge is accompanied by major overshooting. The extension phase (at the instant the stroke occurs) is followed by relatively slow compression leading to major overshoot. In the case of the ascending edge of the exciting signal the situation is just the opposite: first the damper is rapidly compressed (at the instant the stroke occurs), then slowly extended, which is accompanied by minor overshoot. It appears that the overshoot level depends on the MR damper characteristic in the range of high piston velocities during the system response to a step variation of the applied excitation (damper force is lower by nearly 20 N during compression than during extension, leaving aside the force produced by the accumulator).

In the case of algorithm CA1, both for ascending and descending edge of the excitation w_f, the input current i_f^* reaches the maximal value i_m = 0.15 A lasting for about 0.1 s (starting from the moment before the excitation becomes constant), which leads to reduced overshooting.

7. CONCLUSIONS

The paper deals with the experimental study of vibration control in a two-degree-of-freedom pitch-plane suspension model equipped with MR dampers. Operation of standard skyhook and LQ algorithms, also in cooperation with inverse model of MR damper was investigated. The obtained results reveal the advantage in vibration isolation of the feedback systems over the open loop (passive) one.

The best effectiveness for a wide range of excitation frequencies is achieved with the CA3 algorithm, as LQ control delivers optimal (in the aspect of assumed criteria) reference forces response; moreover, inverse model enables to settle appropriate current values. These results are similar to the obtained by the means of numerical analysis.

Authors extended investigated model to the three-degree-of-freedom one introducing additional suspended

mass sub-system representing behaviour of the driver or a cab [6]. Results of those experiments are a subject of other publications.

The implementation of control algorithms on the embedded microcontroller system, as well as model development including consideration of tires dynamics will be investigated.

Acknowledgement

The study is supported through the research fund in 2006–2008 as a research grant No. 4 T07C 016 30.

References

[1] Ahmed A.K.W.: *Encyclopedia of Vibration*. Academic Press, 2002
[2] Karnopp D., Crosby M.J., Harwood R.A.: *Vibration Control Using Semi-Active Force Generators*. Journal of Engineering for Industry, 1974, 619–626
[3] Lai C.Y., Liao W.H.: *Vibration Control of a Suspension System via a Magnetorheological Fluid Damper*. Journal of Vibration and Control, No. 8, c 2002
[4] Marro G., Ntogramatzidis L.: *A contribution to the finite-horizon LQ control*. Incontro in ricordo di Giovanni Zappa, Florencja, Włochy, 2005
[5] Martynowicz P.: *Simulation of a Vehicle Suspension with Magnetorheological Dampers*. Kwartalnik AGH Mechanika, 2003, nr 22, 355–361
[6] Martynowicz P.: *Synteza algorytmów sterowania drganiami dla płaskiego modelu magnetoreologicznego zawieszenia pojazdu*. Ph.D. Thesis, AGH – UST, 2006
[7] Martynowicz P., Sapiński B.: *Pitch-plane Models of MR Vehicle Suspension for Experimental Testing*. Quarterly Mechanics, vol. 24, 2005, 120–123
[8] Nagai M., Onda M., Hasegawa T., Yoshida H.: *Semi-active control of vehicle vibration using continuously variable damper*. 3rd Int. Conf. on Motion and Vibration Control, Chiba, China, 1996, 153–159
[9] Queslati F., Sankar S.: *A class of semi-active suspension schemes for vehicle vibration control*. Journal of Sound and Vibration, 1994, Vol. 172, No. 3, 391–411
[10] Pare C.A., Ahmadian, M.: *Experimental Evaluation of Semiactive Magneto-Rheological Dampers for Passenger Vehicles*. Proc. of 32nd International Symposium on Automotive Technology and Automation (ISATA), Vienna, Austria, 1999
[11] Sapiński B.: *Magnetorheological Dampers in Vibration Control*. AGH-UST Press, 2006
[12] Sapiński B., Martynowicz P.: *Sterowanie liniowo-kwadratowe drganiami w układzie zawieszenia magnetoreologicznego*. Czasopismo Techniczne M/5, Wydawnictwo PK, 2004, 335–343
[13] Sapiński B., Martynowicz P.: *Vibration control in a pitch-plane suspension model with MR shock absorbers*. Journal of Theoretical and Applied Mechanics, 2005, Vol. 43, 655–674
[14] Spencer B., Dyke S., Sain M., Carlson J.: *Phenomenological Model of a Magnetorheological Damper*. ASCE Journal of Engineering Mechanics, March, 1996
[15] Yasuda E., Doi S., Hattori K., Suzuki H., Hayashi Y.: *Improvement of Vehicle Motion and Riding-Comfort by Active Controlled Suspension System*. A Transaction of American Society of Automotive Engineers, No. 910662, 1991
[16] Yokoyama M., Hedrick J.K., Toyama S.: *A Model Following Sliding Mode Controller for Semi-Active Suspension Systems with MR Dampers*. Proc. of the American Control Conference, Arlington, USA, 2001
[17] Zribi M., Karkoub M.: *Robust control of a car suspension system using magnetorheological dampers*. Journal of Vibration and Control, vol. 10, 2004, 507–524